

---

# Near-infrared Laser Computed Tomography of the Breast: First Clinical Experience<sup>1</sup>

Alexander Poellinger, MD, Jan C. Martin, MD, Steven L. Ponder, PhD, Torsten Freund, MD, Bernd Hamm, MD  
Ulrich Bick, MD, Felix Diekmann, MD

---

**Rationale and Objectives.** The purpose of the present study was to evaluate a near-infrared (NIR) laser breast imaging system (Computed Tomography Laser Mammography [CTLM]) as an adjunct to mammography by means of receiver-operating characteristic (ROC) analysis. The NIR technique used in this study is based on the absorption of NIR light by hemoglobin. Malignant tumors can be detected by imaging their neovascularization.

**Materials and Methods.** Eighty-two patients were examined by both CTLM and mammography. Seventy-nine of the 82 patients underwent biopsies, and three patients had 2-year follow up. Three-dimensional scans were acquired with an NIR laser computed tomographic scanner (the CTLM system) at a slice thickness of 4 mm. Mammograms were analyzed alone and together with CTLM images.

**Results.** Histology revealed 37 benign and 42 malignant lesions. For the combination of mammography and CTLM, the area under the ROC curve was significantly larger than for mammography alone. In addition, it was shown that the difference in area under the ROC curve between the combination of both methods and mammography alone was considerably larger for dense breasts than for radiolucent breasts, although these differences were not statistically significant.

**Conclusion.** CTLM, used as an adjunct, may serve as a feasible tool to improve the diagnostic capabilities of mammography.

**Key Words.** Optical tomography; mammography; breast cancer; breast tumors; near infrared imaging

© AUR, 2008

---

Breast cancer is the most frequent malignancy in women worldwide (1–4). Statistically, in the United States, one in seven women will develop breast cancer during her lifetime (5). Diagnostic mammography has been shown to have an average sensitivity for the detection of cancer of 75%, and 60 to 80 of every 100 biopsies are negative for

cancer. In specific cases, magnetic resonance imaging (MRI) can solve some of these problems, increasing sensitivity to about 95%, but with a presently significantly lower specificity than mammography (6). In addition, MRI examinations are still very expensive. For these reasons, a different approach to breast imaging is desirable.

In theory, optical methods based on near-infrared (NIR) imaging have high potential to become valuable diagnostic tools in breast imaging (7,8). There are several reasons for this. First, the breast is fully accessible for imaging with optical methods because of its surface location, relatively small size, and absence of bony structures. Second, at 800 nm, it is possible to exploit the difference in absorption between total hemoglobin and water or fat

---

**Acad Radiol** 2008; 15:1545–1553

<sup>1</sup> From the Department of Radiology, Campus Charité Virchow Klinikum, Augustenburger Platz 1, D-13353 Berlin, Germany (A.P., J.C.M., B.H., U.B., F.D.); Imaging Diagnostic Systems, Inc., Plantation, FL (S.L.P.); and the Department of Informatics, Humboldt University, Berlin, Germany (T.F.). Received June 24, 2008; accepted July 26, 2008. **Address correspondence to:** A.P. e-mail: alexander.poellinger@charite.de

© AUR, 2008

doi:10.1016/j.acra.2008.07.023

as an intrinsic contrast. Hemoglobin will then act as a natural contrast medium, and computed laser tomography of the breast will therefore produce a "hemoglobin angiogram," revealing the normal vascular structures of the breast. In addition, because all tumors require new blood vessels to survive and grow (neovascularization), NIR tomographic imaging can detect tumors within the breast. Third, no ionizing radiation is needed, and the majority of optical systems work without compression, factors that increase its acceptance by patients. Finally, the method is rather inexpensive and easily deployed.

Despite these theoretical advantages, the first research devices based on NIR imaging were mostly disappointing and all less accurate in detecting breast cancer than established imaging methods (9–11). However, considerable advances have been made recently in optical imaging (12–19). We intend to demonstrate the feasibility of a commercially available system (Computed Tomography Laser Mammography [CTLM]; Imaging Diagnostic Systems, Inc., Plantation, FL) to detect neoplastic lesions in the human breast.

## MATERIALS AND METHODS

The study was approved by the institutional review board. Patients provided informed consent to the study.

### Technique

The CTLM scanning mechanism consists of a continuous-wave laser source and an array of 84 collimated photodiodes arranged in third-generation computed tomographic geometry about an aperture that will accommodate most breast sizes (Fig 1). A pair of linear photodiode array cameras is used to map the position of the laser beam on the surface of the breast to the physical location of the beam–breast interface within the scanning chamber, thereby creating an accurate measurement of the breast's perimeter at the interrogated slice.

The laser's wavelength is 808 nm, which is the approximate wavelength in the medical optical spectral window (Fig 2 [20,21]) at which the optical absorptions of oxyhemoglobin and deoxyhemoglobin are equivalent (22). At this wavelength, the primary contrast absorber in breast tissue is hemoglobin (both oxyhemoglobin and deoxyhemoglobin) (23), allowing CTLM to produce images of all blood-containing structures, both normal and abnormal, within the breast.

During the CTLM procedure, the patient lies prone on the table with one breast pendant in the scanning cham-

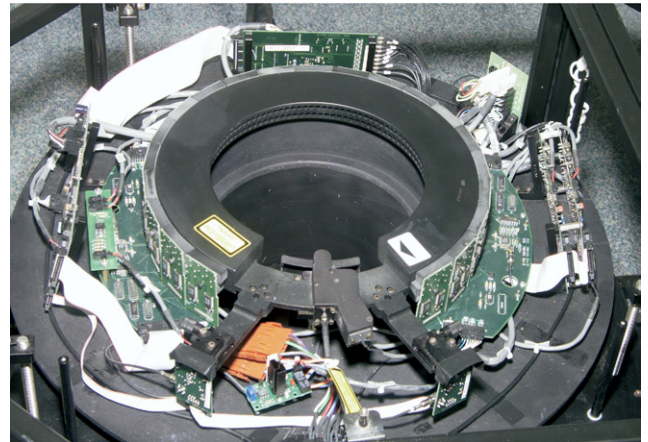


**Figure 1.** Gantry of the Computed Tomography Laser Mammography system using a third-generation computed tomography design. There is an array of 84 collimated photodiodes and a near-infrared laser operating at 808 nm.

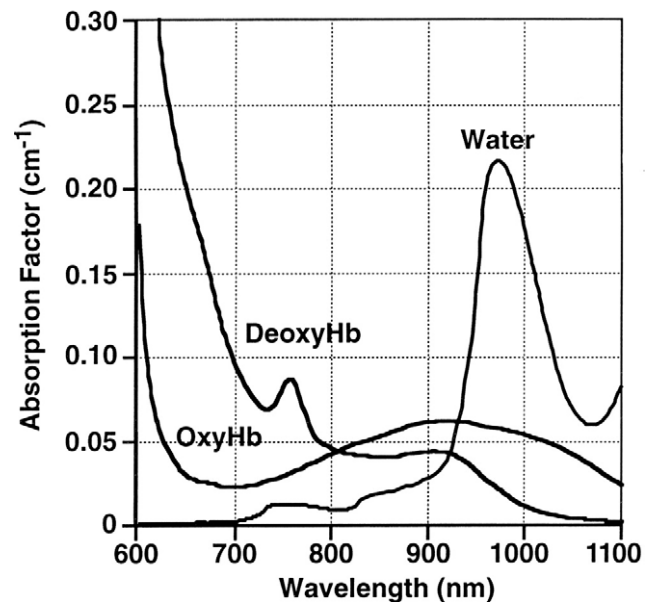


**Figure 2.** Medical optical spectral window demonstrated by the absorption spectra of the major chromophores in skin (20,21). The absorption factor is equivalent to the optical absorption coefficient,  $\mu_a$ . OxyHb, oxyhemoglobin; DeoxyHb, deoxyhemoglobin. (From Chance (21), with permission).

ber. The CTLM exam is a free-space measurement: there is no coupling medium between the scanning gantry and the breast, and no part of the scanning mechanism contacts the breast. The scanning mechanism rotates 360°, initially in a plane near the chest wall, and measures the light diffused by the breast at a number of views in a single slice. After completing its rotation, the scanning mechanism automatically descends a predetermined dis-

tance and acquires the next contiguous slice of data. This procedure is repeated until the end of the breast is encountered. The average time required to scan one breast, using a standard slice spacing of 4 mm, is 12 minutes.

Reconstruction of the CTLM images is performed slice by slice. Using the diffusion approximation of the transport equation (24), an estimate of the average optical absorption is computed for each slice (the "forward model") using the data collected by the collimated photodiodes and the measured perimeter. The forward model is compared to the measured data to extract the equivalent of an x-ray computed tomographic fan-beam measurement of the absorbing perturbations in the slice. These perturbation data are then reconstructed into slice images using a highly modified proprietary filtered back-projection algorithm that converts the fan-beam data into standard computed tomographic (sinographic) data, corrects for geometric distortions due to bulk light-tissue interaction, and compensates for a spatially variant blurring effect that is typical of diffuse optical imaging (25,26).

The contiguous individual reconstructed slices for a single breast scan are combined to form a volumetric data set using standard processing techniques. The CTLM system's image display software provides interactive viewing of both multiplanar reconstructions and volumetrically rendered representations of the distribution of total hemoglobin throughout the breast.

For the majority of cases in this study, the slice thickness was set to 4 mm, with acquisition times varying from 10 to 25 minutes depending on the size of the breast.

## Patients

Eighty-two patients were included in this study, 79 of whom had unclear lesions on mammography, ultrasound, or MRI or had palpable masses on physical examination (see Table 1). Seventy-nine patients were biopsied after their NIR scans were performed.

Three patients with benign findings were not biopsied but were still included in the study because they had 2-year mammographic follow-up. Patients' ages ranged from 30 to 90 years (mean, 56.3; standard deviation, 12.4 years). All patients had undergone mammography within the past 2 months. Exclusion criteria were (1) bloody discharge, ulcers, or wounds of the breast; (2) a biopsy or breast surgery had been performed within the 6 months before the optical tomography; and (3) the patient was undergoing current irradiation of the breast or chemotherapy.

**Table 1**  
**Seventy-nine of 82 Patients Included in This Study Had Biopsies on the Basis of Findings on Mammography, Ultrasound, Magnetic Resonance Imaging, Physical Examination, or a Combination of These Methods; Three Patients with Benign Findings Were Included on the Basis of 2-Year Follow-up**

Basis for Biopsy	Number of Patients
Mammography	47
Ultrasound	5
Mammography and ultrasound	7
Physical examination and mammography	10
MRI	5
Physical examination and ultrasound	2
Physical examination and MRI	2
Mammography and MRI	1

MRI, magnetic resonance imaging.

## Analysis

On the basis of our own observations and earlier studies (27), we determined that there are only two normal vascularized structures in the breast that are visible on CTLM: (1) blood vessels (veins and arteries), which appear as tubular structures, frequently anastomosing with other blood vessels, widening from the nipple to the base but with some "flattening" due to the reconstruction algorithm, giving a ribbonlike appearance; and (2) pyramidal structures, which match with the location of lobes. There are therefore only two normal shapes on CTLM studies: tubular and pyramidal.

Any structure that appears on a CTLM image (and therefore contains blood) that is not tubular or pyramidal must be read as abnormal and is usually caused by some form of angiogenesis. This angiogenic structure is frequently, but not invariably, very "bright" (white) on the CTLM study. However, there is considerable variation in the vascularity of tumors depending on their histologic types and stages and on their sizes. Tumors larger than 1.5 cm begin to outgrow their blood supply and necrose in the center, causing a decrease in vessel count. The diagnosis of an angiogenic structure is therefore made as frequently from its abnormal shape as from its intensity.

The most common shapes for angiogenesis to assume include (1) roughly spherical (on rotation, the three-dimensional image does not flatten out), (2) ovoid, (3) fusiform, (4) saccular, and (5) discoid (convex-concave).

## Reading Mammograms and CTLM Studies

First, the 82 mammograms were read alone. The lesion with the highest level of suspicion for malignancy was

**Table 2**  
**Histologic Findings in the 79 Patients Who Were Biopsied;**  
**There Were 42 Malignant Cases in Total**

Finding	Number of Lesions	Size (mm), Mean ± SD
Malignant findings		16.7 ± 14.1
Invasive ductal carcinoma	29	
Invasive lobular carcinoma	4	19.3 ± 7.0
Mucinous carcinoma	1	10
High-grade DCIS	6	22.4 ± 23.9
Low-grade DCIS	2	36.5 ± 47.4
Benign findings		
Fibrocystic changes	12	
Fibrosis	9	
Fibroadenoma	7	17.0 ± 11.0
Benign calcifications	3	
Papilloma	2	
Atypical ductal hyperplasia	2	
Hamartoma	1	
Chronic mastitis	1	
Follow-up	3	

DCIS, ductal carcinoma in situ; SD, standard deviation.

evaluated on a scale ranging from 0 to 100. After 3 weeks, mammograms and NIR images were read in conjunction. The reader was asked first to record the position of the lesion of greatest suspicion on the mammogram and then to determine whether one or more of the aforementioned morphologic forms of angiogenesis were present on the NIR image. Using the presence or absence of angiogenesis on the NIR image, the reader was then asked to reassess the level of suspicion, on the basis of both the mammogram and the CTLM image. Receiver-operating characteristic (ROC) curves were then plotted for the mammography-only readings and for the mammography-plus-CTLM readings using the ROCKIT 0.9B program (Charles E. Metz, University of Chicago, Chicago, IL).

**Statistical Analysis**

Differences between the areas under the ROC curves (AUCs) for the mammography-alone readings and the mammography-plus-CTLM readings were evaluated using the  $\chi^2$  test. A *P* value < .05 was considered significant. In addition, differences in the ROC curves were evaluated with regard to different breast densities.

**RESULTS**

**Histology**

Histology in 79 patients and 2-year follow-up in three patients revealed 42 malignancies (51%) and 37 benign

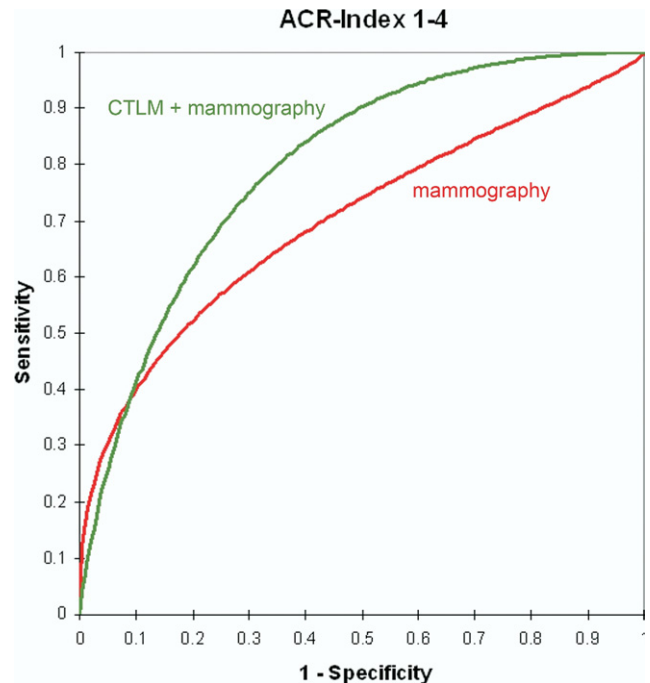


**Figure 3.** Receiver-operating characteristic (ROC) curve analysis between mammography and Computed Tomography Laser Mammography (CTLM) plus mammography. The bivariate  $\chi^2$  statistic of the difference between the two ROC estimates was statistically significant, with a corresponding *P* value of .033. ACR, American College of Radiology.

lesions (45%) (Table 2). The malignant lesions included 29 invasive ductal carcinomas (69%), four lobular carcinomas (10%), one mucinous carcinoma (2%) and eight ductal carcinomas in situ (six high grade, two low grade) (19%). The benign lesions consisted of 12 fibrocystic mastopathies (30%), nine fibroses (23%), seven fibroadenomas (18%), two papillomas (5%), two atypical ductal hyperplasias (5%), one hamartoma (2%), one chronic mastitis (2%), and three microcalcifications (8%) without any changes of the glandular tissue.

**Mammography**

The mammographic lesions were classified as masses (*n* = 49), calcifications (*n* = 21), combinations of masses and microcalcifications (*n* = 9), architectural distortions (*n* = 2), and asymmetry (*n* = 1).

**Statistical Analysis**

ROC curve analysis revealed AUCs (mean ± standard error) for all breast densities of 0.722 ± 0.056 for mammography alone and 0.796 ± 0.049 for mammography plus CTLM, resulting in a difference in AUC of 0.07 (Fig 3).

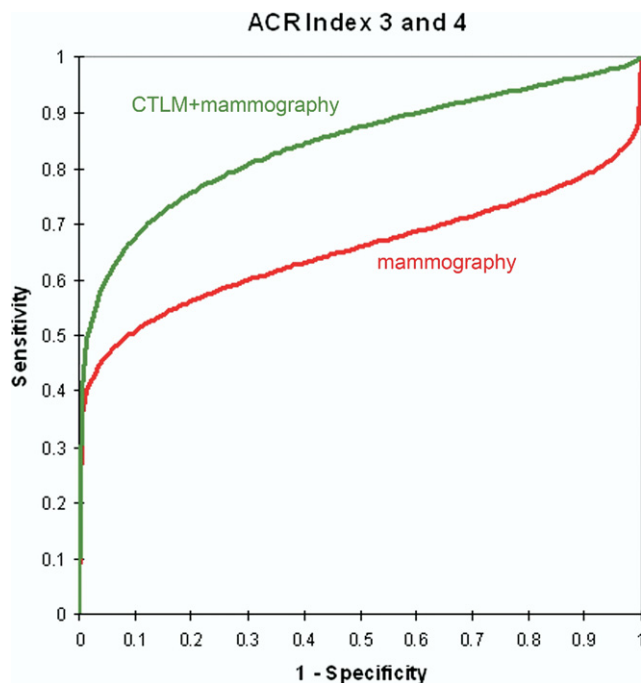


**Figure 4.** For radiographically dense breasts, the difference between the area under the receiver-operating characteristic curve was even greater. However, mainly because of the smaller number of patients in this subset, the difference did not reach statistical significance ( $\chi^2$  test,  $P = .073$ ). ACR, American College of Radiology; CTLM, Computed Tomography Laser Mammography.

The bivariate  $\chi^2$  test of the difference between the two ROC curve estimates was statistically significant, with a corresponding  $P$  value of .033.

Thirty-eight of the 82 cases were classified as American College of Radiology Breast Imaging Reporting and Data System (BI-RADS) density 3 or 4. For this subset of dense breasts, the improvement in the ROC curves was even greater. The AUCs were  $0.644 \pm 0.092$  for mammography alone and  $0.831 \pm 0.070$  for mammography plus CTLM, a difference of 0.186 (Fig 4). However, because of the smaller number of patients in this subset, the bivariate  $\chi^2$  test of the difference between the two ROC curve estimates was not statistically significant, with a corresponding  $P$  value of .073.

Forty-four cases were classified as BI-RADS density 1 or 2. For this subset, the AUCs were  $0.740 \pm 0.074$  for mammography alone and  $0.761 \pm 0.072$  for mammography plus CTLM (Fig 5). The difference in AUC (0.018) was not statistically significant. The bivariate  $\chi^2$  test of the difference between the two ROC curve estimates yielded a  $P$  value of .205.

Mammography in combination with CTLM correctly identified seven of the eight ductal carcinomas in situ and two of the four lobular carcinomas. Seven of 13 false-

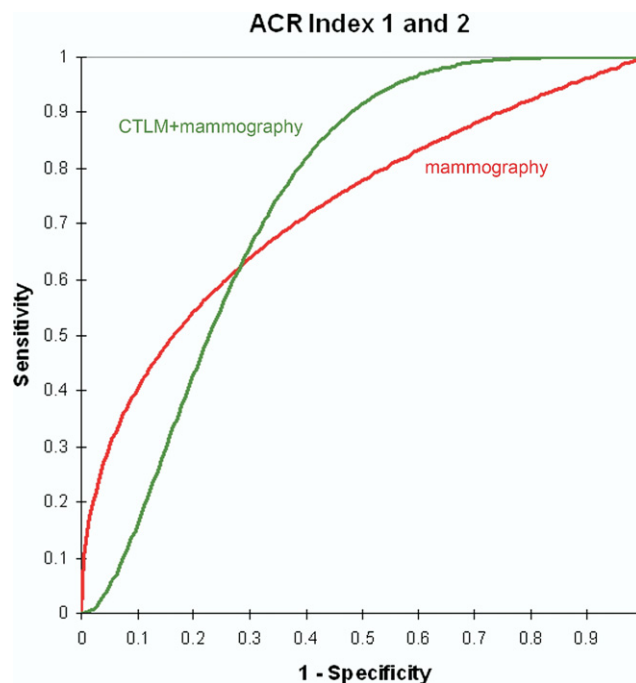


**Figure 5.** The difference in the area under the receiver-operating characteristic curve between mammography and the combination of Computed Tomography Laser Mammography (CTLM) and mammography was not statistically significant for radiolucent breasts (American College of Radiology [ACR] Breast Imaging Reporting and Data System density 1 or 2).

positive lesions (resulting from the mammography-plus-CTLM readings) were caused by benign focal lesions.

## Cases

In this section, we describe three patients with varying types of malignancy to illustrate some particular facets of CTLM imaging.

### Case 1: Ductal Carcinoma in Situ and Invasive Ductal Carcinoma

A 28-year-old patient presented with a palpable lesion in her left breast. Mammography showed a spiculated mass at 12 o'clock that was highly suspicious for breast cancer (BI-RADS grade 5). On the CTLM image, there was a circumscribed area of hypervascularity at 12 o'clock. Dynamic MRI provided a good correlation with the CTLM image (Fig 6). Histology revealed an invasive ductal carcinoma and a high-grade ductal carcinoma in situ (overall tumor size, 30 mm).

### Case 2: Invasive Ductal Carcinoma

A patient presented with a mass at 12 o'clock in the right breast. Mammography showed architectural distortion in this

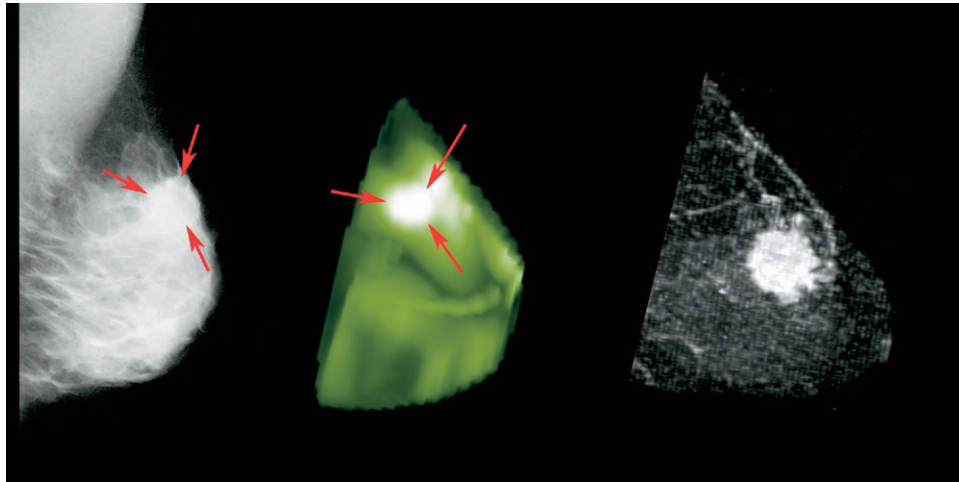


**Figure 6.** Correlation between mammography, Computed Tomography Laser Mammography, and magnetic resonance imaging in a 28-year-old woman with an invasive ductal carcinoma and ductal carcinoma in situ (high grade) in her left breast.

### Case 3: Cystosarcoma Phyllodes and Fibroadenoma

A 54-year-old postmenopausal patient presented with a palpable mass in her left breast. An MRI examination revealed a large, well-circumscribed, and apparently encapsulated heterogeneous mass in the inner upper quadrant that was  $37 \times 36 \times 53$  mm in size. On T<sub>2</sub>-weighted images, the tumor appeared mostly hyperintense. (Histologically, this was a cystosarcoma phyllodes tumor.) Lateral to this tumor, a smaller, less hyperintense, and more homogeneous mass,  $23 \times 23 \times 31$  mm in size, was observed (Fig 8). (Histologically, this was a fibroadenoma). Following MRI, we performed a CTLM examination. Using CTLM, only the malignant mass was observed (Fig 8). The benign mass did not show angiogenesis on CTLM.

Confirming the CTLM findings, immunohistologic examination using cluster of differentiation 31, a marker for endothelial cells, demonstrated a low degree of vascularization in the smaller tumor (Fig 9b) and dense tumor microvascularization in the larger mass (Fig 9d).

**Figure 7.** Correlation between mammography and Computed Tomography Laser Mammography (CTLTM) showing an invasive ductal carcinoma. On mammography, a architectural distortion at 12 o'clock was present. The CTLM images show a hyperintensity (white arrows) indicating hypervascularity.

area, which could be appreciated only on the craniocaudal films (Fig 7). CTLM showed a distinct area of hypervascularization, corresponding with the tumor. Histology revealed an invasive ductal carcinoma (tumor size, 14 mm).

## DISCUSSION

In this preliminary study, we found that the combination of a commercially available continuous-wave NIR laser mammographic system (CTLTM) and mammography is more accurate than mammography alone. There was a statistically significant increase in the AUC (difference, 0.07;  $P = .033$ ) for mammography plus CTLM compared with mammography alone. In

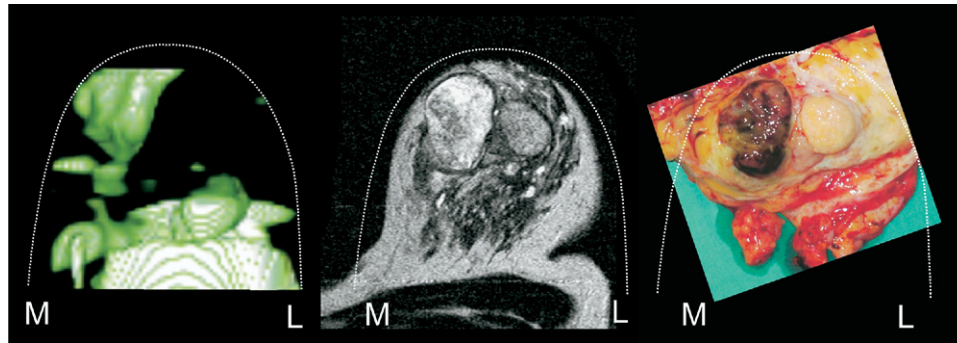


**Figure 8.** Comparison of near-infrared mammography (Computer Tomography Laser Mammography [CTL M], three-dimensional surface rendering) (*left*), magnetic resonance imaging (MRI; T<sub>2</sub>-weighted) (*center*), and the operation specimen (*right*). Both CTL M and MRI showed the larger mass that was located medially (M). The smaller mass, located laterally (L), was seen only on MRI and did not appear on near-infrared mammography. Histologic examination revealed a malignant phyllodes tumor as the larger mass and a fibroadenoma as the smaller mass. The structures at the base of the breast in the near-infrared image are probably caused by large vessels and dense glandular tissue.

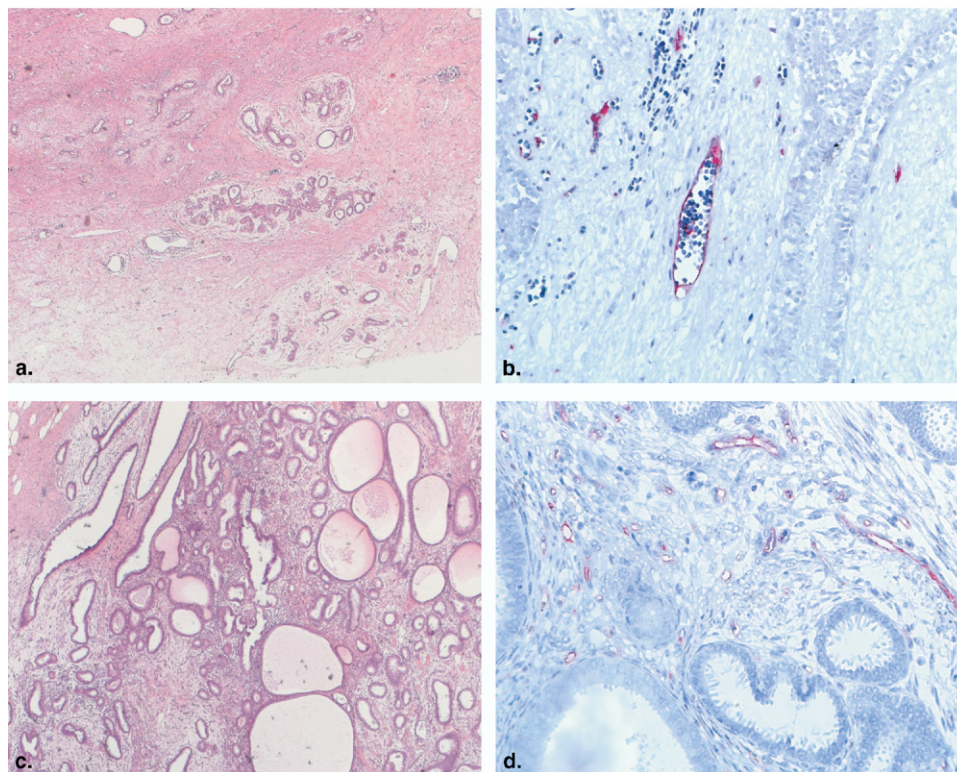


**Figure 9.** (a) Fibroadenoma with proliferation of stromal cells around ducts (25 ×, hematoxylin and eosin). (b) Immunohistochemical staining showing moderate intratumoral vascularization by cluster of differentiation 31 (CD31) (200 ×, alkaline phosphatase antialkaline phosphatase). (c) Malignant phyllodes tumor with dense spindle-cell stroma (25 ×, hematoxylin and eosin). (d) Immunohistochemical staining demonstrating dense intratumoral vascularization by CD31 (200 ×, alkaline phosphatase antialkaline phosphatase).

radiographically dense breasts (BI-RADS density 3 and 4), an even greater (0.19) increase in the AUC was achieved. However, because of the smaller number of patients in this subset, the difference did not reach sta-

tistical significance. In patients with radiolucent breast tissue (BI-RADS density 1 and 2), there was only a slight increase in AUC of 0.02, which was also not statistically significant.

To our knowledge, this is the first study to evaluate an NIR scanner in combination with mammography by ROC analysis. Because we tested the combination of an NIR scanner and mammography instead of the NIR scanner alone, there might be bias in interpreting the results, but our approach best reflects a clinical scenario in which an NIR scanner would be used as an adjunct to mammography. In addition, a study evaluating the feasibility of CTLM alone has already been performed by Floery et al (27). In their study, they showed that malignant lesions were detected significantly more often by CTLM than benign ones. However, they concluded that at that point, using CTLM as a single modality would not suffice for breast cancer detection (27).

In addition to their study, there have been many NIR studies in recent years. Compared to established techniques (mammography, MRI), none of these studies has shown an acceptable detection rate for breast cancers by NIR imaging when used as a single modality (28,29). However, in combination with mammography, promising results have been achieved (29–32). Although optical methods lack spatial resolution, it is possible to measure chromophores, such as hemoglobin, fat, and oxygen, which is not feasible with other methods such as mammography (for the present study, the wavelength in the CTLM device was set up only to measure total hemoglobin). In the future, using both spatial information by mammography and physiologic information by NIR imaging, increased accuracy is achievable. Using contrast agents such as indocyanine green or more modern ones that are currently applicable only for animal studies (33), a further increase in diagnostic accuracy might be feasible (34).

Eleven of the 83 cases were false-positives on mammography, and 14 cases were false-positives on mammography plus CTLM. Of the cases that were positive on mammography plus CTLM but not on mammography, three were benign neoplastic lesions, such as fibroadenomas and papillomas. In total, of the 14 false-positive cases on mammography plus CTLM, seven lesions were associated with higher neovascularization (three fibroadenomas, two papillomas, one hamartoma, and one mastitis). A certain percentage of benign lesions will show some angiogenesis (33). This phenomenon is well known from magnetic resonance mammography and is the main reason for its rather low specificity. In total, seven lesions were picked up by CTLM although there was no focal lesion present. Also, by MRI, we learned that there are some benign non-neoplastic structures that show increased enhancement. Some of them are fibrocystic changes. We

hypothesize that NIR imaging also depicts these changes as increased absorption by NIR light. Other groups have also reported the rather low specificity of optical methods (35–37). This is not surprising, because benign focal lesions have a higher microvessel density compared to surrounding tissue (38).

### Study Limitations

Limitations of the present study include the reading of mammograms without supplementary information, the rather small number of cases, and a possible bias in the statistics because of the mixture of cases used in the study. The mammograms were read without the benefit of patient histories or prior diagnostic results. Moreover, only the breast bearing a possible lesion was read, so information obtained by comparison with the opposite breast was not used. This approach probably lowered the accuracy of mammographic reads. Eighty-two cases are certainly not enough to fully evaluate the ability of a new system to differentiate between benign and malignant cases; however, the aim of this study was to demonstrate the feasibility of the system, not to evaluate it as a diagnostic technique to be compared to other current diagnostic standards.

The rather low AUC for mammography alone (0.722) points to the fact that malignant neoplasms in our mammographic set were harder to detect by mammography alone, compared to other studies (39) with reported AUCs of 0.75 and higher.

We intentionally did not include breast ultrasound as an adjunct to mammography, although it is the first-line imaging modality to combine with mammography. As a feasibility study, this study aimed to clarify differences between mammography and the combination of mammography and CTLM. Further studies are needed to compare combinations of methods, such as mammography and ultrasound versus mammography and CTLM.

### Conclusion

We have demonstrated that computed tomographic laser mammography, used as an adjunct, is a feasible tool to improve the diagnostic capabilities of mammography. The improvement in diagnostic accuracy for the combination of mammography and CTLM compared to mammography alone was statistically significant. The diagnostic improvement shown in this small series using CTLM as an adjunct to mammography needs to be confirmed in a larger study.

## REFERENCES

- Parkin DM, Fernandez LM. Use of statistics to assess the global burden of breast cancer. *Breast J* 2006; 12(suppl):S70–S80.
- Bray F, McCarron P, Parkin DM. The changing global patterns of female breast cancer incidence and mortality. *Breast Cancer Res* 2004; 6:229–239.
- Parkin DM, Bray F, Ferlay J, Pisani P. Global cancer statistics, 2002. *CA Cancer J Clin* 2005; 55:74–108.
- Smigal C, Jemal A, Ward E, et al. Trends in breast cancer by race and ethnicity: update 2006. *CA Cancer J Clin* 2006; 56:168–183.
- Jemal A, Siegel R, Ward E, et al. Cancer statistics, 2008. *CA Cancer J Clin* 2008; 58:71–96.
- Saslow D, Boetes C, Burke W, et al. American Cancer Society guidelines for breast screening with MRI as an adjunct to mammography. *CA Cancer J Clin* 2007; 57:75–89.
- Gibson AP, Hebden JC, Arridge SR. Recent advances in diffuse optical imaging. *Phys Med Biol* 2005; 50:R1–R43.
- Hielscher AH. Optical tomographic imaging of small animals. *Curr Opin Biotechnol* 2005; 16:79–88.
- Ntziachristos V, Chance B. Probing physiology and molecular function using optical imaging: applications to breast cancer. *Breast Cancer Res* 2001; 3:41–46.
- Drexler B, Davis JL, Schofield G. Diaphanography in the diagnosis of breast cancer. *Radiology* 1985; 157:41–44.
- Brenner RJ. X-ray mammography and diaphanography in screening for breast cancer. *J Reprod Med* 1982; 27:679–684.
- Grosenick D, Moesta KT, Moller M, et al. Time-domain scanning optical mammography: I. Recording and assessment of mammograms of 154 patients. *Phys Med Biol* 2005; 50:2429–2449.
- Taroni P, Torricelli A, Spinelli L, et al. Time-resolved optical mammography between 637 and 985 nm: clinical study on the detection and identification of breast lesions. *Phys Med Biol* 2005; 50:2469–2488.
- Srinivasan S, Pogue BW, Jiang S, et al. In vivo hemoglobin and water concentrations, oxygen saturation, and scattering estimates from near-infrared breast tomography using spectral reconstruction. *Acad Radiol* 2006; 13:195–202.
- Zhou C, Choe R, Shah N, et al. Diffuse optical monitoring of blood flow and oxygenation in human breast cancer during early stages of neoadjuvant chemotherapy. *J Biomed Opt* 2007; 12:051903.
- Ntziachristos V, Yodh AG, Schnall M, Chance B. Concurrent MRI and diffuse optical tomography of breast after indocyanine green enhancement. *Proc Natl Acad Sci U S A* 2000; 97:2767–2772.
- Corlu A, Choe R, Durduran T, et al. Diffuse optical tomography with spectral constraints and wavelength optimization. *Appl Opt* 2005; 44:2082–2093.
- Alacam B, Yazici B, Chance B, Nioka S. Characterization of breast tumors with NIR methods using optical indices. *Conf Proc IEEE Eng Med Biol Soc* 2007; 1:5186–5189.
- Alacam B, Yazici B, Intes X, Nioka S, Chance B. Pharmacokinetic-rate images of indocyanine green for breast tumors using near-infrared optical methods. *Phys Med Biol* 2008; 53:837–859.
- O'Leary MA. *Imaging with diffuse photon density waves*. Philadelphia, PA: University of Pennsylvania Press; 1996.
- Chance B. Near-infrared images using continuous, phase-modulated, and pulsed light with quantitation of blood and blood oxygenation. *Ann N Y Acad Sci* 1998; 838:29–45.
- Torricelli A, Spinelli L, Pifferi A, Taroni P, Cubeddu R, Danesini G. Use of a nonlinear perturbation approach for in vivo breast lesion characterization by multiwavelength time-resolved optical mammography. *Opt Express* 2003; 11:853–867.
- Nioka S, Chance B. NIR spectroscopic detection of breast cancer. *Technol Cancer Res Treat* 2005; 4:497–512.
- Star WM. Diffusion theory of light transport. In: Welch AJ, van Gemert MJC, eds. *Optical-thermal response of laser-irradiated tissue*. New York: Plenum Press; 1995:131–206.
- Grable RJ, Rohler DP, Sastry KLA. Optical tomography breast imaging. *Proc SPIE* 1997; 2979:197–210.
- Rohler DP, Sastry KLA, Ross S. Method for reconstructing the image of an object scanned with a laser imaging apparatus. US Patent #6,130,958; 2000.
- Floery D, Helbich TH, Riedl CC, et al. Characterization of benign and malignant breast lesions with computed tomography laser mammography (CTLM): initial experience. *Invest Radiol* 2005; 40:328–335.
- Grosenick D, Wabnitz H, Moesta KT, et al. Concentration and oxygen saturation of haemoglobin of 50 breast tumours determined by time-domain optical mammography. *Phys Med Biol* 2004; 49:1165–1181.
- Franceschini MA, Moesta KT, Fantini S, et al. Frequency-domain techniques enhance optical mammography: initial clinical results. *Proc Natl Acad Sci U S A* 1997; 94:6468–6473.
- Pogue BW, Poplack SP, McBride TO, et al. Quantitative hemoglobin tomography with diffuse near-infrared spectroscopy: pilot results in the breast. *Radiology* 2001; 218:261–266.
- Shah N, Cerussi A, Eker C, et al. Noninvasive functional optical spectroscopy of human breast tissue. *Proc Natl Acad Sci U S A* 2001; 98:4420–4425.
- Cerussi AE, Berger AJ, Bevilacqua F, et al. Sources of absorption and scattering contrast for near-infrared optical mammography. *Acad Radiol* 2001; 8:211–218.
- Weissleder R. Molecular imaging in cancer. *Science* 2006; 312:1168–1171.
- Intes X, Ripoll J, Chen Y, Nioka S, Yodh AG, Chance B. In vivo continuous-wave optical breast imaging enhanced with Indocyanine Green. *Med Phys* 2003; 30:1039–1047.
- Boehm T, Hochmuth A, Malich A, Reichenbach JR, Fleck M, Kaiser WA. Contrast-enhanced near-infrared laser mammography with a prototype breast scanner: feasibility study with tissue phantoms and preliminary results of imaging experimental tumors. *Invest Radiol* 2001; 36:573–581.
- Tomandl B, Doinghaus K, Schulz-Wendtland R. Laser mammography with near-infrared light. *Rontgenpraxis* 1995; 48:197–201.
- Gotz L, Heywang-Kobrunner SH, Schutz O, Siebold H. Optical mammography in preoperative patients. *Aktuelle Radiol* 1998; 8:31–33.
- Wells WA, Daghighian CP, Tosteson TD, et al. Analysis of the microvasculature and tissue type ratios in normal vs. benign and malignant breast tissue. *Anal Quant Cytol Histol* 2004; 26:166–174.
- Pisano ED, Gatsonis C, Hendrick E, et al. Diagnostic performance of digital versus film mammography for breast-cancer screening. *N Engl J Med* 2005; 353:1773–1783.